remote sensing

MDPI

Article

Insights into Spatiotemporal Variations in the NPP of Terrestrial Vegetation in Africa from 1981 to 2018

Qianjie Wang [1], Liang Liang [1,*], Shuguo Wang [1], Sisi Wang [2], Lianpeng Zhang [1], Siyi Qiu [1], Yanyan Shi [1], Jin Shi [1] and Chen Sun [1]

[1] School of Geography, Geomatics and Planning, Jiangsu Normal University, Xuzhou 221116, China
[2] National Remote Sensing Center of China, Beijing 100036, China
* Correspondence: liang_rs@jsnu.edu.cn; Tel.: +86-187-9623-7312

Abstract: The net primary productivity (NPP) of vegetation is an important indicator used to evaluate the quality of terrestrial ecosystems and characterize the carbon balance of ecosystems. In this study, the spatiotemporal distribution and dynamic change in NPP in Africa from 1981 to 2018 were analyzed using the long time series data of NPP. The results of the trend and fluctuation analysis showed that the NPP in the Sahara arid region in northern Africa and the arid region in South Africa exhibited a significant reduction and a high degree of fluctuation; most of the NPP in the tropical rainforests in central Africa and the deciduous broadleaved forests and deciduous needle-leaved forests on the north and south sides of the tropical rainforests increased and showed a low degree of fluctuation; the Congo basin, Gabon, Cameroon, Ghana, Nigeria, Tanzania, and other regions were affected by human activities, while the NPP in these regions exhibited a significant reduction and a high degree of fluctuation. Anomaly analysis showed that the NPP in Africa generally exhibited a slow upward trend during the period from 1981 and 2018. The trend was basically consistent in different seasons, and can be segmented into three phases: (1) a phase of descent from 1981 to 1992, with the NPP below the average value in most years; (2) a phase of steady growth from 1993 to 2000, reaching a peak in 2000; (3) a phase of fluctuations from 2001 to 2018, where the NPP value was above the average value in all years except 2015 and 2016, when the NPP value was low due to abnormally high temperatures and drought. The Mann–Kendall test further showed that the annual and seasonal NPP in Africa exhibited a significant upward trend, and the mutation time points occurred around 1995. The wavelet time series analysis revealed obvious periodic changes in the time series of NPP in Africa. The annual and seasonal NPP showed clear oscillations on time scales of 7, 20, 29, and 55 years. The 55-year period had the strongest signal, and was the first main period. The study can provide a scientific gist for the sustainable development of environmental ecology, agricultural production, and the social economy in Africa.

Keywords: carbon sink; NPP; Africa; trend analysis; coefficient of variation; Mann–Kendall mutation test; time series; wavelet analysis

Citation: Wang, Q.; Liang, L.; Wang, S.; Wang, S.; Zhang, L.; Qiu, S.; Shi, Y.; Shi, J.; Sun, C. Insights into Spatiotemporal Variations in the NPP of Terrestrial Vegetation in Africa from 1981 to 2018. *Remote Sens.* **2023**, *15*, 2748. https://doi.org/10.3390/rs15112748

Academic Editors: Yuhong He, Adrian Ursu, Cristian Constantin Stoleriu, Justin F Moat and Marian Mierlă

Received: 24 February 2023
Revised: 20 May 2023
Accepted: 22 May 2023
Published: 25 May 2023

1. Introduction

The net primary productivity (NPP) of vegetation refers to the amount of organic substance accumulated by vegetation per unit area in a given period of time [1]. NPP reflects the ability of plants to fix and convert inorganic carbon into organic carbon using sunlight for photosynthesis. It indicates the production capacity of vegetation communities under natural conditions and represents the quality of terrestrial ecosystems, and it is also the main factor characterizing the carbon sources and sinks of ecosystems and plays an important role in global carbon cycle research [2]. Therefore, the International Biological Program (IBP) proposed by UNESCO, Global Change and Terrestrial Ecosystems (GCTE), and the International Geosphere-Biosphere Program (IGBP) have all identified the NPP research of global terrestrial vegetation as one of their core contents [3].

NPP acquisition methods mainly include site observation methods, experimental methods, and model-based methods [4]. Early site observation or experimental methods provide basic parameters and verification data for model construction, but the data obtained are point source data with poor real-time performance. The model-based method can address the shortcomings of the above methods [5]. Models for estimating NPP mainly include statistical models (such as Miami [6] and Chikugo [7]), process models (such as CENTRY [8] and BIOME-BGC [9]), and light utilization models (such as CASA [10] and GLO-PEM [11]). These models require many input variables to characterize vegetation characteristics and combine environmental factors to estimate global or regional NPP. With the rapid development of remote sensing technology, large-scale target areas can be observed periodically and frequently, creating favorable conditions for quantifying the spatiotemporal characteristics of model parameters and making the model estimation method driven by remote sensing data the mainstream method for large-scale NPP estimation [12–14]. The relevant research included the construction of the model, the calibration and optimization of model parameters, the coupling and improvement of different models, and the application of different models to achieve a simulated estimation of NPP on different scales [15–17].

Ghaderpour et al. [18] used wavelet analysis to conduct spatiotemporal monitoring of land cover and climate, showing the coherency and phase delay between vegetation and climate. Aalijahan et al. [19] used the Mann–Kendall (MK) test to analyze spatiotemporal variations and mutations in precipitation and climate. Liang et al. [20] analyzed the spring vegetation drought conditions in China by taking the vegetation condition index (VCI) as an indicator using the MK method and wavelet analysis. With the accumulation of NPP estimation data, the National Earth System Science Data Center (NESSDC), National Science & Technology Infrastructure of China, released global NPP datasets of 500 m from 2000 to 2020 and 5 km from 1981 to 2018. It is possible to analyze the spatial and temporal distribution and dynamic changes in NPP between years and to evaluate the environmental quality, ecological processes, and carbon balance of a researched regional ecosystem [21–26].

In recent years, the environmental problems of land desertification, deforestation, and wetland resource reduction in Africa (especially in the sub-Saharan region) have become increasingly serious and have attracted global attention. Most regions of Africa are ecologically fragile and vulnerable to irreversible environmental degradation due to climate change [27]. Therefore, although Africa has the lowest greenhouse gas emissions of all continents (except Antarctica), African ecosystems rank first in terms of the worst effects of climate change on ecosystem stability. The report of the United Nations Development Programme (UNDP) pointed out that CO_2 and other greenhouse gases emitted by developed countries will have a serious impact on Africa, especially the sub-Saharan region, in the future [28]. Therefore, it is important to determine how to use NPP and other indicators to monitor and assess the ecological environment in Africa and provide data support and knowledge services for its sustainable development.

The growth of vegetation in Africa can be analyzed by studying the spatiotemporal distribution pattern and dynamic change in long-term NPP. In this study, we used the long time series data of global NPP from 1981 to 2018 released by the NESSDC to meet the following research goals: (1) analyze the correlation between the spatial distribution pattern of NPP and its land cover type in Africa; (2) use trend analysis, the anomaly index, and the Mann–Kendall mutation test to study the changing trend and mutation time of NPP in different seasons; (3) use coefficient of variation to analyze the fluctuation degree of NPP in different seasons; and (4) use wavelet analysis to explore the periodic changes and temporal patterns of NPP in different seasons. Analyzing NPP in this fashion provides a basis for the sustainable development of environmental ecology, agricultural production, and the social economy in Africa.

2. Study Region and Data

2.1. Study Region

Africa lies in the western portion of the eastern hemisphere, bordered by the Indian Ocean to the east and the Atlantic Ocean to the west, and is the second largest continent in the world. The desert area of Africa accounts for approximately 1/3 of the whole continent, and the Sahara Desert is the largest desert in the world. For the convenience of research, according to the latest United Nations Geographical Program of the Statistics Division of the United Nations Department of Economic and Social Affairs, Africa is divided into North Africa and Sub-Saharan Africa. Sub-Saharan Africa is divided into Central Africa, East Africa, South Africa, and West Africa [29–31] (Figure 1).

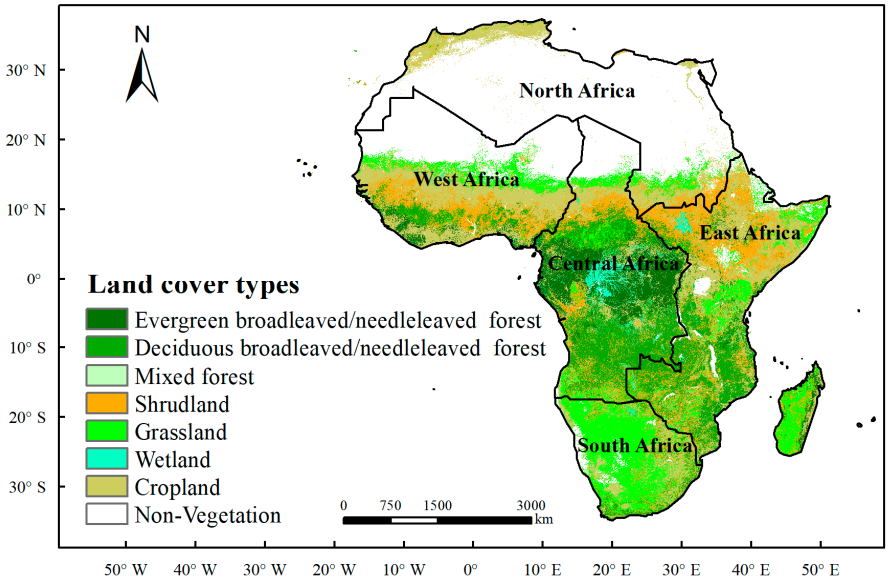

Figure 1. Study area. The background is land cover types.

The equator traverses the middle of the African continent, and three quarters of Africa lies between the Tropics of Cancer and Capricorn. There are four main climate characteristics of Africa: high temperature and heat all year round, vast area with drought and little rain, uneven distribution of precipitation among regions, and symmetrical distribution of climate zones from north to south with the equator as the center. The climate of Africa is characterized by obvious zonality and symmetry, and the distribution of African vegetation also shows strong zonality and symmetry. Tropical rainforests are distributed in the Congo Basin near the equator and along the coast of the Gulf of Guinea, and basically extend to 5° north and south latitudes. The tropical rainforest belt extends to the south and north, and the vegetation type gradually becomes deciduous broadleaved forest, deciduous needleleaved forest, shrub, grassland, and so on as precipitation gradually becomes scarcer. These vegetation types are typical of those in Africa. Grassland vegetation grows well in the rainy season, but in the dry season, precipitation is scarce, and the grassland degrades to yellow and dry. Grasslands are distributed both north and south of the equator, and the northern part of the grasslands to the north of the equator is a tropical desert zone characterized by high temperature, drought, and little vegetation.

2.2. Research Data

2.2.1. NPP Dataset and Preprocessing

The NPP data source was based on GLASS FPAR and LAI data, MODIS global 5 km land-use coverage products, and ERA Interim meteorological data, produced by using the light energy utilization model MuSyQ-NPP; the algorithm introduced the Clearness Index (CI) to improve the LUE estimate, resulting in NPP data from January 1981 to December 2018 [32,33]. The data were acquired from the NESSDC (http://www.geodata.cn) [34]. The

spatial resolution of the image was 5 km and the temporal resolution was 8 days. There were 46 imaging scans in a whole year.

To better study the global terrestrial vegetation NPP, it was essential to compute the average annual NPP over four seasons utilizing the above-mentioned dataset. First, the maximum value composite (MVC) was used for monthly NPP value generation. This treatment can reduce the influences of the clouds, atmosphere, sensor observation geometry, and solar altitude angles on NPP data. According to the seasonal division of meteorology on the solar calendar, the average NPP of the four seasons was defined as the cumulative average NPP of the corresponding months of their seasons. Finally, the annual average NPP was defined as the cumulative average NPP in spring, summer, autumn, and winter. Then, the global NPP time-series data of the year and four seasons from 1981 to 2018 were obtained and finally cut according to the vector file of Africa.

2.2.2. Land Cover Data and Preprocessing

Land cover data are taken from a free, shared global land cover remote sensing data product (GlobCover 2009) [35]. This product was produced by the European Space Agency (ESA) based on the Envisat Medium Resolution Imaging Spectrometer (MERIS) sensor, using high-quality image data from January to December 2009 with a resolution of 300 m. GlobCover products use the LCCS classification system of the Food and Agriculture Organization of the United Nations (FAO), which divides global land cover types into 22 categories. In this study, excessive land cover objects were reasonably merged to form 8 types of land cover type systems.

3. Research Methods

To analyze the spatiotemporal distribution and dynamic variation in NPP in Africa, we implemented trend analysis, coefficient of variation analysis, anomaly analysis, the Mann–Kendall mutation test, and wavelet analysis on the long-term time series data of NPP in Africa from 1981 to 2018. The methods used were as follows.

3.1. NPP Trend Analysis

To analyze the variation trends of NPP according to the NPP values of each pixel from 1981 to 2018, the following formula was used to calculate the trend rate [36,37]:

$$slope = \frac{n \times \sum_{i=1}^{n} (i \times NPP_i) - \sum_{i=1}^{n} i \sum_{i=1}^{n} NPP_i}{n \times \sum_{i=1}^{n} i^2 - \left(\sum_{i=1}^{n} i \right)^2} \quad (1)$$

where i is the serial number from 1981 to 2018 (1–38), n is the total length of the time series (n = 38), and NPP_i is the NPP value in year i. Additionally, $slope > 0$ suggested the NPP value exhibited an uptrend during the research period; otherwise, it exhibited a downtrend.

The F test method was applied to define the significance of the change trend. The data follow the F distribution with $(1, n-2)$ degrees of freedom, where n represents 38 years. Based on the F distribution table, when the significance levels were 95% and 99%, the critical values were 4.113 and 7.396, that is, $F_{0.05(1,38)} = 4.113$ and $F_{0.01(1,38)} = 7.396$. Based on the values of the F test and slope, the trend analysis result was segmented into five levels (Table 1).

Table 1. Different variation levels of NPP determined by trend analysis and F test.

Slope of Average NPP	F Test Value	Variation Grade of NPP
slope > 0	$F \geq 7.396$	Significantly increased
	$4.113 \leq F < 7.396$	Increased
	$F < 4.113$	No significant change
slope < 0	$F < 4.113$	
	$4.113 \leq F < 7.396$	Reduced
	$F \geq 7.396$	Significantly reduced

3.2. NPP Volatility Analysis

The coefficient of variation (CV) was applied to analyze the degree of volatility of the NPP in Africa from 1981 to 2018. The larger the value is, the greater the fluctuation of the NPP and the more unstable it is in the time series, and vice versa, for overall stability [36,38]. The calculation formula is [36]:

$$CV = \frac{stdev}{\overline{NPP}} \tag{2}$$

$$stdev = \sqrt{\frac{\sum_{i=1}^{n} \left(NPP_i - \overline{NPP}\right)^2}{n-1}} \tag{3}$$

where *stdev* is the NPP standard deviation and $\overline{NPP}$ is the average NPP in the research period.

To reflect the changes in NPP in Africa more intuitively, the CV value was divided into five grades [39] (Table 2).

Table 2. Different fluctuation degrees of NPP defined by the coefficient of variation.

CV Value	Fluctuation Degree of NPP
$CV \leq 0.1$	Less fluctuation
$0.1 < CV \leq 0.2$	Low fluctuation
$0.2 < CV \leq 0.3$	Moderate fluctuation
$0.3 < CV \leq 0.4$	High fluctuation
$CV > 0.4$	Very high fluctuation

3.3. Anomaly NPP

Anomaly NPP is defined as the difference between the value of NPP in a certain period of a specific year and the average value of NPP over a period of many years, and is mainly utilized to analyze the historical changes of NPP. The definition of the anomaly NPP is as follows [40]:

$$NPP_{\mathrm{a}} = \frac{NPP_i - \overline{NPP}}{\overline{NPP}} \tag{4}$$

where NPP_{a} is the NPP anomaly. A positive NPP_{a} indicates that the NPP value of the current year is higher than the average annual value, while a negative NPP_{a} indicates that the NPP value of the current year is lower than the average annual value.

3.4. Mann–Kendall Mutation Test

To test whether there was a mutation during the study period, the Mann–Kendall mutation test was performed on the NPP dataset. The Mann–Kendall test is a non-parametric statistical test, also known as the non-distribution test, which has the advantage of not requiring samples to follow a certain distribution and not being disturbed by a few outliers [41]. This method is usually combined with trend analysis to determine the mutation point and significance level of the change trend, and has been widely used in hydrology, meteorology, vegetation analysis, etc. [42]. The calculation formula is [43]:

$$UF_k = \frac{[s_k - E(s_k)]}{\sqrt{Var(s_k)}}, (k = 1, 2, \ldots, n) \quad (5)$$

where $s_k = \sum_{i=1}^{k} r_i$ and r_i are the number of samples that are between 1 and i and are less than x_i. Under the null assumption, the mean and variance are as follows:

$$E(s_k) = \frac{n(n-1)}{4} \quad (6)$$

$$Var(s_k) = \frac{n(n-1)(2n+5)}{72} \quad (7)$$

The process was duplicated for the inverse time series to compute UB_k. Then, UB_k and UF_k were plotted in MATLAB with a 0.05 ($U_{0.05} = \pm 1.96$) confidence interval. This method can effectively determine whether the time series are in a condition of natural stochastic fluctuation or have a certain tendency. Values of UB_k or UF_k higher than zero represent an uptrend; otherwise, they indicate a downtrend. If UB_k or UF_k exceed the confidence interval of 0.05, the change trend reaches a significant level; if there is an intersection between the two in the confidence interval between −1.96 and 1.96, the time point can be considered as a mutation point. If there are multiple intersections close together inside the confidence interval or the intersections appear outside the confidence interval, it is necessary to combine this approach with other test methods to further determine whether the intersections are mutation points [19,44,45]. The advantage of this method is that it is simple to calculate. It can also identify the time of mutation onset and point out the mutation region. Therefore, it is a common method of mutation detection.

3.5. Wavelet Analysis

For the study of time series, time domain analysis and frequency domain analysis are two basic forms of analysis. Among them, time domain analysis can be used for time location, but not to obtain more information about the changes of time series; the frequency domain analysis has the function of accurate frequency location, but it is only suitable for stationary time series analysis. However, most time series belong to non-stationary series, which not only have the characteristics of tendency and periodicity, but also have the characteristics of randomness, mutation, and "multi-time scale" structure. Because of the traits of multiresolution analysis, wavelet analysis can reflect the signal's local features in the frequency and time domains. Thus, this method can acquire the waveform of the time series by resolving the time series into the time-frequency domain [46]. In the early 1980s, a wavelet with a time-frequency multi-resolution function was proposed by Morlet to balance the localization of time and frequency. It can reveal a variety of variation cycles hidden in the time series and reflect the variation trends of the system in different scales [47]. Therefore, the Morlet wavelet is used in this paper to analyze the periodic change pattern of NPP in Africa from 1981 to 2018. A continuous Morlet wavelet is defined as [18]:

$$\varphi(\mathrm{t}) = \pi^{-\frac{1}{4}} e^{-iw_0 t} e^{-\frac{t^2}{2}} \quad (8)$$

where $\pi^{-\frac{1}{4}}$ is a standardized factor to ensure unit variance, the Morlet wavelet, $\varphi(\mathrm{t})$, is the result of sine complex $e^{-iw_0 t}$ and Gaussian wave package $e^{-\frac{t^2}{2}}$, t is the dimensionless time, and w_0 is the dimensionless frequency [18,48].

4. Results and Analysis

4.1. NPP Distribution Pattern in Africa

Figure 2 shows the average NPP of Africa from 1981 to 2018. The figure indicates that the spatial distribution pattern of NPP in Africa was highly related to its land cover type. It was basically centered at the equator and distributed symmetrically toward the poles, and with the increase in latitude, the NPP gradually decreased.

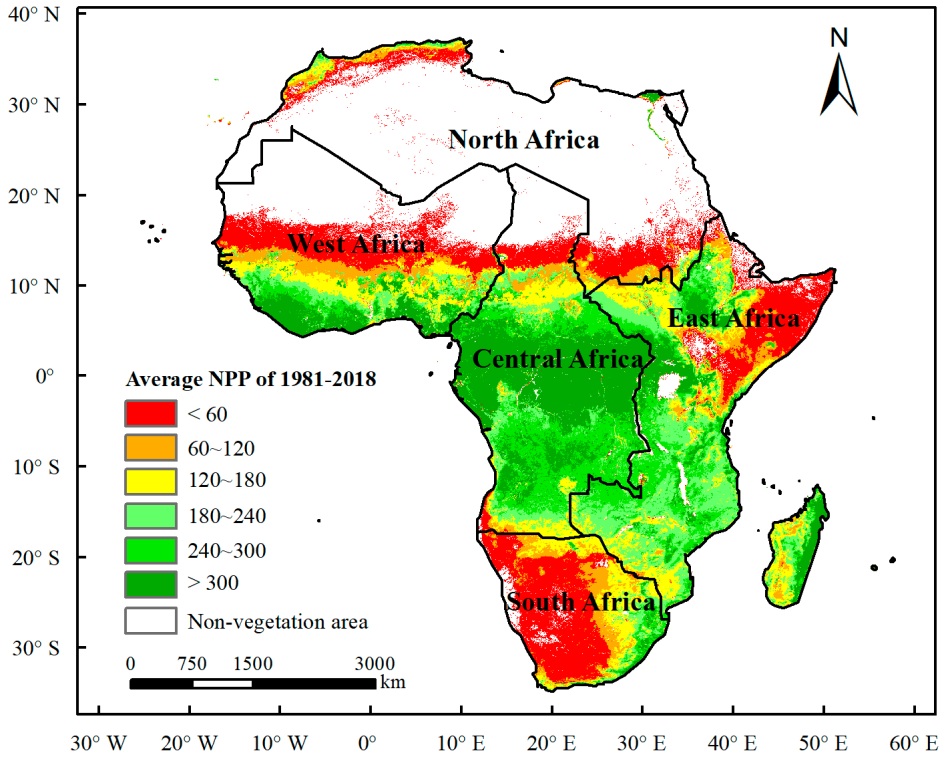

Figure 2. Spatial distribution of average NPP of 1981–2018 in Africa.

The high-value area (>300 gC·m^{-2}·a^{-1}) of NPP in Africa was chiefly distributed in the tropical rainforest belt, which is centered on the equator and extends approximately 5° from north to south and 30°E from west to east, mainly including the center of central Africa and southern West Africa. The NPP of the region was much higher than that of other regions because of its lush vegetation, hot and humid conditions, and rainy conditions. The medium-value area (180~300 gC·m^{-2}·a^{-1}) of NPP was chiefly located in the north and south sides of the Central African tropical rainforest, the north side of the West African tropical rainforest and the south side of East Africa, and mainly consisted of deciduous broadleaved forest, deciduous needle-leaved forest, and mixed forest. The southern Sahara Desert, eastern East Africa and most of South Africa were low value areas (<180 gC·m^{-2}·a^{-1}), mainly grassland, cropland, and shrubland belts. In South Africa, the NPP decreased from east to west, mainly because the warm water vapor along the coast is affected by the southeast trade wind and the humidity decreases gradually from east to west, leading to a gradual decrease in precipitation. The Sahara Desert to the north of 15°N (most of North Africa, northern Central Africa, and West Africa) has no vegetation or very little vegetation, and the NPP of vegetation was close to zero.

4.2. NPP Trend Analysis in Africa

The F test and trend analysis were utilized to study the trends of the annual (Figure 3) and seasonal (Figure 4) NPP in Africa from 1981 to 2018, and the distinct trend grades of the NPP were calculated.

The annual NPP exhibited a significant change trend and was more representative than the seasonal NPP, with a total of 46% of the regional NPP change. The NPP decreased in 24% of the area (20% of which reached a significant level), mainly concentrated in the grassland, cropland, and shrubland south of the Sahara Desert. The NPP increased in 22% of the areas (17% of which reached a significant level), mainly in the tropical rainforest and the deciduous broadleaved forests and needle-leaved forests on its north and south sides. This is because the tropical rainforest has an equatorial rainy climate with ample rainfall throughout the year. However, the change trend of wetlands in tropical rainforests was

not significant, and the NPP in sporadic areas decreased, which may have been caused by excessive human logging activities in these areas.

To better reflect the seasonal variation in NPP in Africa over 38 years, the NPP variation trends of the four seasons in Africa over 38 years were analyzed (Figure 4, Table 3). The regions with decreasing trends in the four seasons were far more abundant than those with increasing trends. The NPP in the tropical rainforest area exhibited a growth trend in the four seasons because the tropical rainforest is in the equatorial rainy climate, with sufficient rainfall throughout the year and without an obvious dry or wet season. The shrubland, cropland, and grassland in the north of the tropical rainforest exhibited a declining trend in the four seasons, but the declining trend in spring and winter was more obvious than that in summer and autumn. The growth trend of NPP in deciduous forests and grasslands in southern tropical rainforests in spring and winter was also more obvious than that in summer and autumn. Although the north and south of the tropical rainforest are in the tropical dry and wet season climate, the change trend of NPP in different seasons was inconsistent, which may be owing to the huge discrepancy in topography between the north and south.

Table 3. Percentage of NPP in different grades of variation in different seasons.

Change Level of NPP	Spring	Summer	Autumn	Winter
Significantly reduced	23%	18%	18%	21%
Reduced	5%	6%	7%	5%
No significant change	53%	59%	56%	51%
Increased	6%	5%	5%	6%
Significantly increased	14%	11%	14%	16%

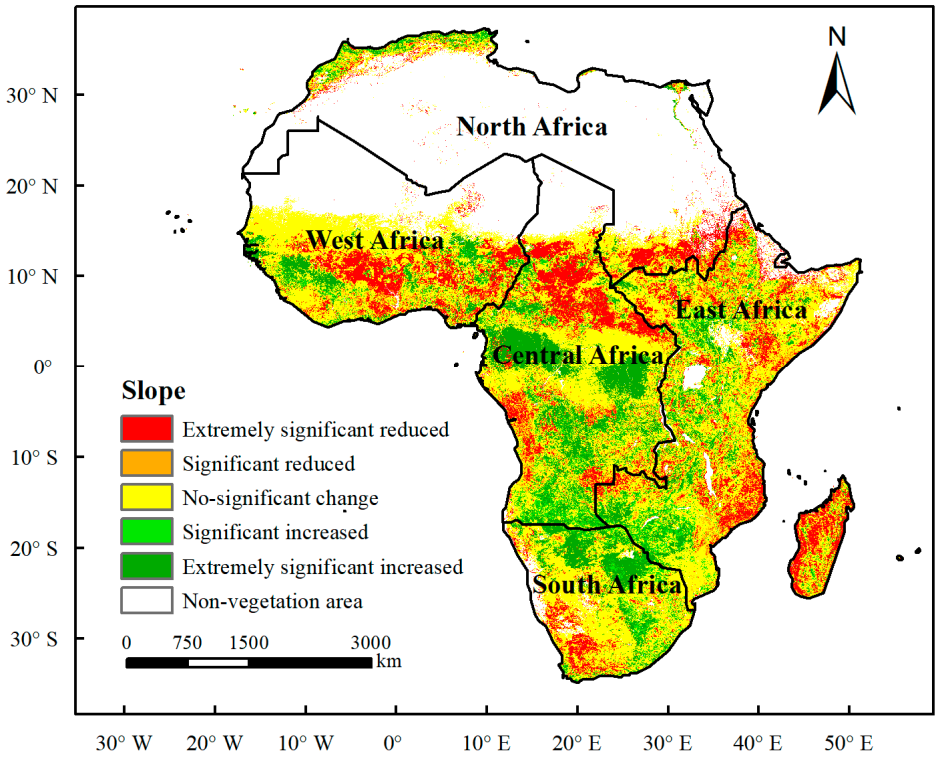

Figure 3. Slope trend analysis results of the annual average NPP from 1981–2018 in Africa (significantly increased: *slope* > 0 & F ≥ 7.396; increased: *slope* > 0 & 4.113 ≤ F < 7.396; no significant change: F < 4.113; reduced: *slope* < 0 & 4.113 ≤ F < 7.396; significantly reduced: *slope* < 0 & F ≥ 7.396).

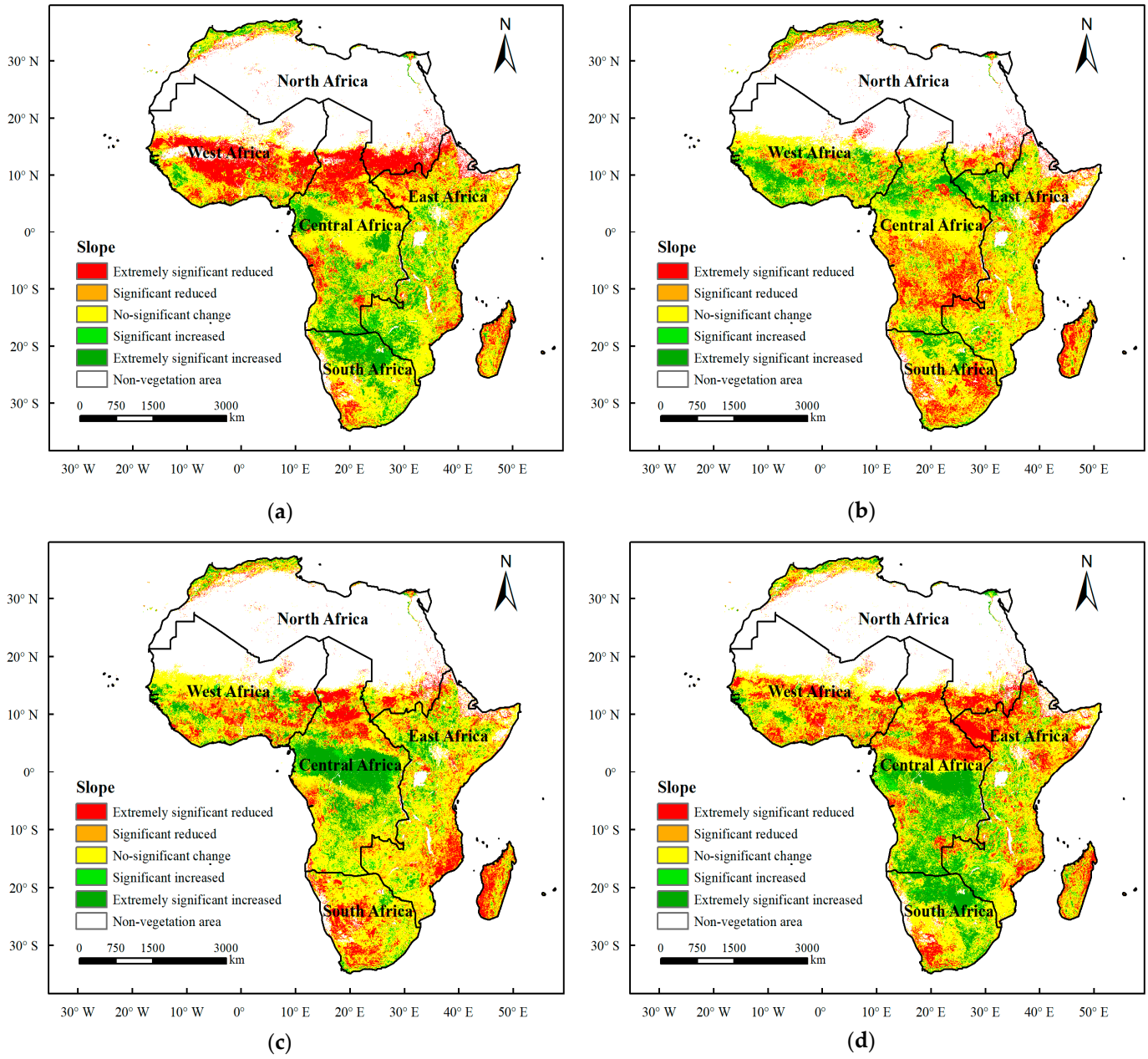

Figure 4. Slope trend analysis results of average NPP from 1981–2018 in the spring (**a**), summer (**b**), autumn (**c**), and winter (**d**) (significantly increased: *slope* > 0 & F ≥ 7.396; increased: *slope* > 0 & 4.113 ≤ F < 7.396; no significant change: F < 4.113; reduced: *slope* < 0 & 4.113 ≤ F < 7.396; significantly reduced: *slope* < 0 & F ≥ 7.396).

4.3. Volatility Analysis of NPP in Africa

The degrees of annual (Figure 5) and seasonal (Figure 6) fluctuations in Africa from 1981 to 2018 were analyzed using the coefficient of variation.

The level of fluctuation of the annual NPP was more representative than that of seasonal NPP. Overall, 63% of the regions had a low degree of NPP fluctuation, mainly concentrated in the equatorial tropical rainforest region and its northern and southern sides, and the tropical rainforest region had the lowest NPP fluctuation. Comparing the map of land cover types in Africa, we found that the areas with low fluctuation degrees were mainly evergreen broadleaved and needle-leaved forest and deciduous broadleaved and needle-leaved forest. Only 25% of the regions had a high degree of fluctuation in NPP, and were mainly concentrated in the Sahara arid region and South Africa arid region.

Comparing the map of land cover types in Africa, we found that grassland had the highest degree of fluctuation.

To reflect the fluctuation of NPP in Africa in more detail, the fluctuation degree of NPP in the four seasons in Africa over 38 years was analyzed (Figure 6, Table 4). The NPP fluctuations in spring and winter were roughly similar. The areas with high fluctuations were mainly concentrated in the north of 5°N and South Africa, and the regions with low fluctuations were mainly concentrated between 20°S and 5°N. The NPP fluctuations in summer and autumn also had something in common. The regions with high fluctuations were chiefly concentrated in the Sahara Desert to the north of 15°N, eastern East Africa, and South Africa, and the areas with low fluctuations were chiefly concentrated in the tropical rainforest, with the equator as the center, extending approximately 5° to the north and south and extending from the west to the east to 30°E.

Table 4. The percentage of NPP in different fluctuation degrees in different seasons.

Fluctuation Degree of NPP	Spring	Summer	Autumn	Winter
Less fluctuation	26%	17%	20%	25%
Low fluctuation	19%	29%	21%	20%
Moderate fluctuation	13%	23%	20%	14%
High fluctuation	9%	12%	15 %	13%
Very high fluctuation	32%	20%	24%	29%

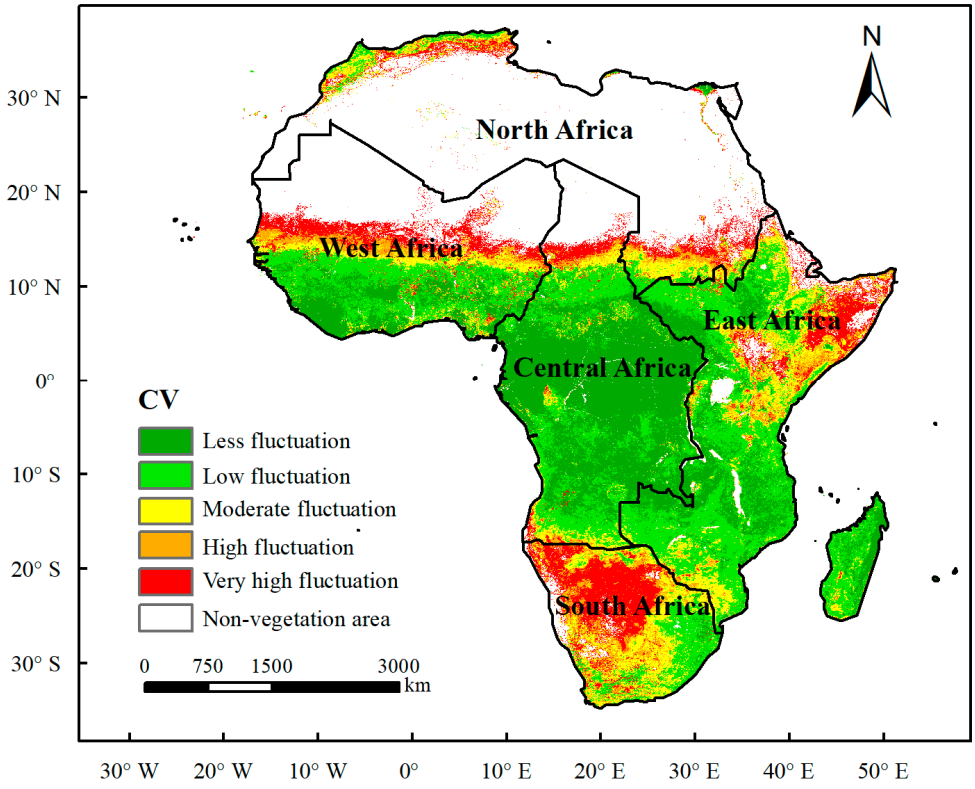

Figure 5. Degree of fluctuation of the annual average NPP from 1981 to 2018 in Africa (less fluctuation: CV $\leq$ 0.1; low fluctuation: 0.1 < CV $\leq$ 0.2; moderate fluctuation: 0.2 < CV $\leq$ 0.3; high fluctuation: 0.3 < CV $\leq$ 0.4; very high fluctuation: CV > 0.4).

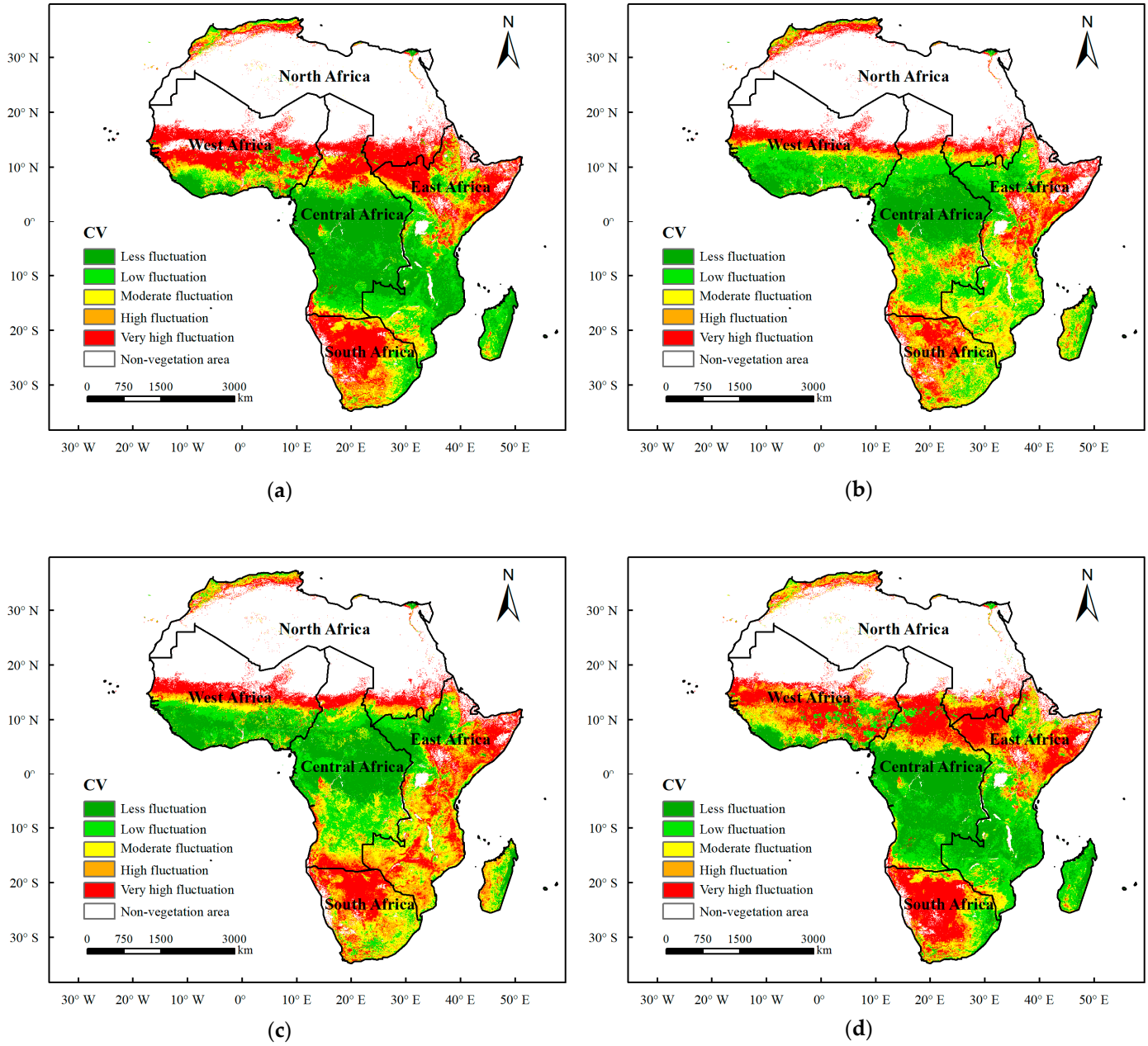

Figure 6. Degree of fluctuation of average NPP from 1981 to 2018 in the spring (**a**), summer (**b**), autumn (**c**), and winter (**d**) (less fluctuation: CV $\leq$ 0.1; low fluctuation: 0.1 < CV $\leq$ 0.2; moderate fluctuation: 0.2 < CV $\leq$ 0.3; high fluctuation: 0.3 < CV $\leq$ 0.4; very high fluctuation: CV > 0.4).

4.4. NPP Temporal Features in Different Seasons

To study the temporal features of NPP in Africa, the anomaly NPP during different seasons from 1981 to 2018 was analyzed (Figure 7). As seen from the figure, the NPP in Africa rose slowly from 1981 to 2018, and the trends in different seasons were basically consistent. Particularly, the stage from 1981 to 2018 can be segmented into three phases. During 1981–1992, the NPP showed a downward trend, and in most years, the NPP was below the mean value, indicating that Africa's carbon sink capacity was low at this stage. Specifically, the NPP declined significantly during the period from 1987 to 1992, which was associated with global cooling and La Niña during this period and was influenced by the eruption of Pinatubo in 1991. The NPP grew steadily from 1993 to 2000 and reached its peak in 2000, indicating that Africa's carbon sink capacity was strong at this stage. The NPP fluctuated from 2001 to 2018 and was higher than the average in most years.

One of the characteristics of the El Niño phenomenon in Africa in 2015 and 2016 was the long-term high temperature [49], which led to abnormally high temperature and drought, thus causing the NPP to be lower than average.

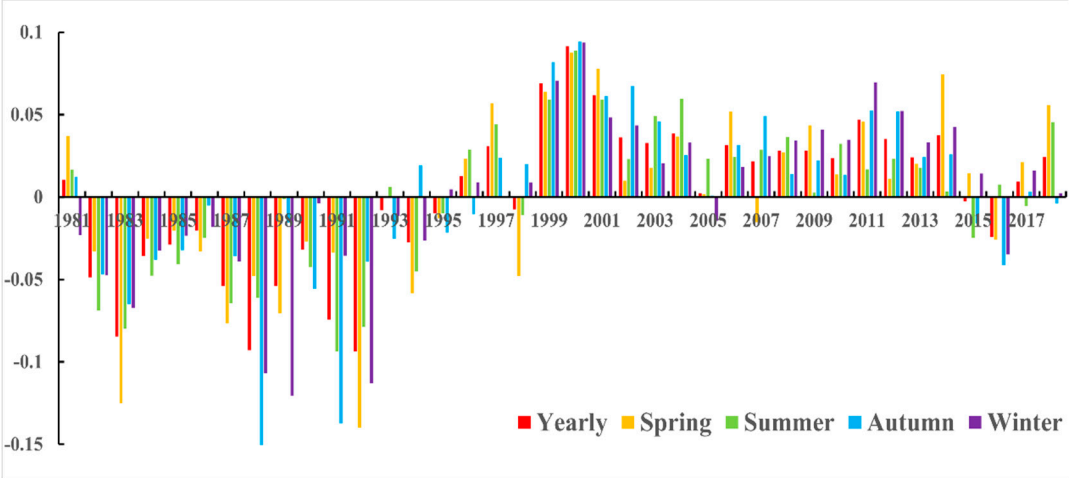

Figure 7. Interannual changes in anomalous NPP during different seasons.

4.5. Mutation Analysis of NPP Time Series in Different Seasons

The Mann–Kendall test was utilized to effectively determine whether the temporal changes in the NPP time series were the result of natural stochastic fluctuation or exhibited obvious tendency. The UB and UF statistics of the NPP from 1981 to 2018 in Africa for each season were computed. Their curves with a confidence interval of 0.05 ($U_{0.05} = \pm 1.96$) were drawn in MATLAB.

According to Figures 8 and 9, most UF curves of the year and seasons were above zero, indicating that the annual and seasonal NPP grew with time. The curves of UF and UB intersected in 1994 and passed the 0.05 significance level in 1999, indicating that the annual NPP showed a significant upward trend and that there was a mutation point in 1994 (Figure 8). The UF and UB curves of NPP in the four seasons of spring, summer, autumn, and winter had only one mutation point within the confidence interval, which occurred in 1995, 1992, 1993 and 1994, while the curves all exceeded the 0.05 level (Figure 9). This indicates that the seasonal mutations all occurred around 1995, which is consistent with the anomaly analysis results described in Section 4.4.

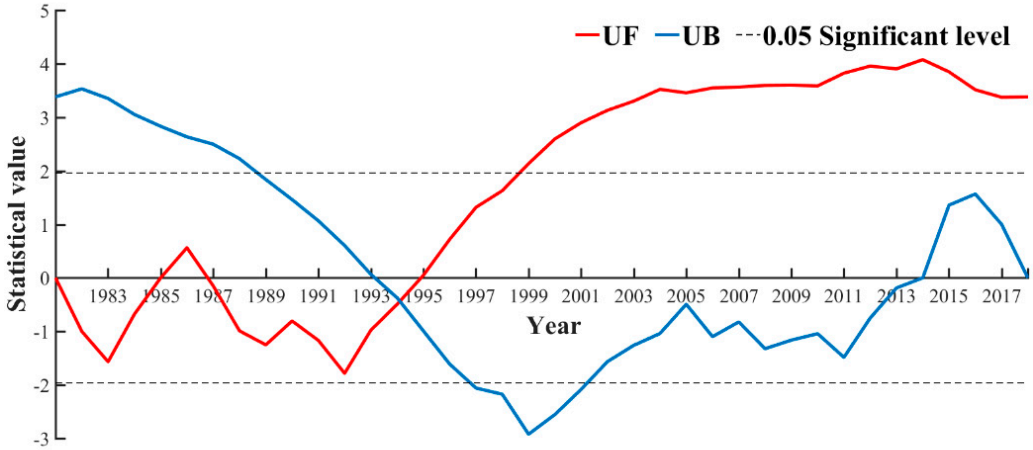

Figure 8. Mutation analysis results of annual NPP from 1981 to 2018.

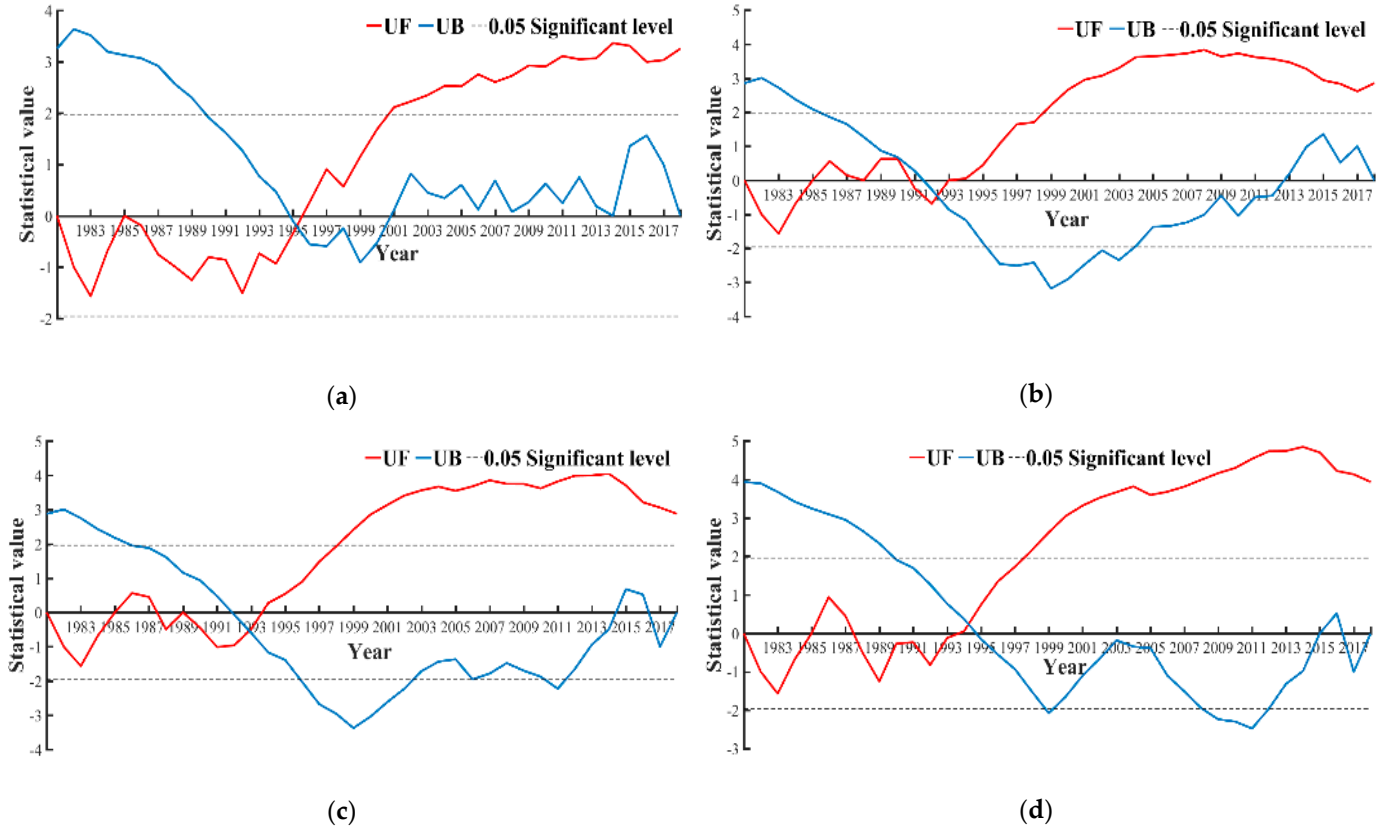

Figure 9. Mutation analysis results of NPP from 1981 to 2018 in the spring (**a**), summer (**b**), autumn (**c**) and winter (**d**).

4.6. Wavelet Analysis of the NPP

Figure 10 is the result of analyzing African NPP time series changes using the Morlet wavelet. The wavelet coefficient graph reflects the periodic variations at different time scales in the time series and can predict the variations pattern of African NPP; the wavelet variance graph can reflect the wavelet energy distribution at different time scales and can be used to identify the main phase in the course of variation. The variance and contour graph of the wavelet coefficients indicates that there were clearly short periods of 5 to 8 years and 18 to 22 years and long periods of 25 to 33 years on the annual scale. Combined with the wavelet variance graph, we found evident oscillations on the time scales of 7, 19, and 28 years. Among them, the signal in the 28-year period was the strongest, which was the first primary period, while the second and third periods were 19-year and 7-year periods.

To study the variation in NPP in different seasons, the NPP of four seasons in Africa was analyzed (Figure 11). As in the case of the annual scale, we found that the four seasons had obvious oscillations on the time scales of 7 years, 19 years, and 28 years with the wavelet variance graph of the seasonal scale. The first main cycle and annual scale of NPP in spring, summer, and autumn were the same, 28 years. Among them, the second and third cycles of autumn were also consistent with the annual scale, while spring and summer were exactly the opposite. Specifically, the first main period of winter was 19 years, while the second and third periods were 28 and 7 years, respectively.

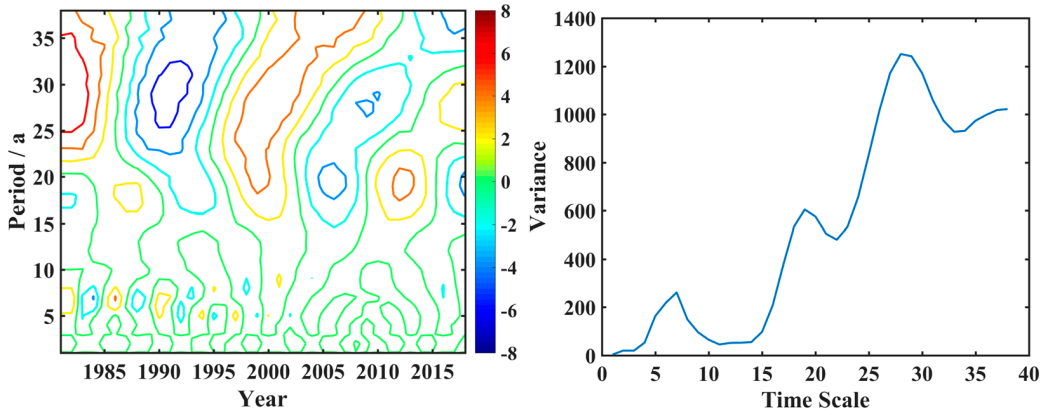

Figure 10. Wavelet time series analysis of NPP in Africa, 1981–2018. The wavelet coefficient contour map (**left**) and wavelet variance graph (**right**).

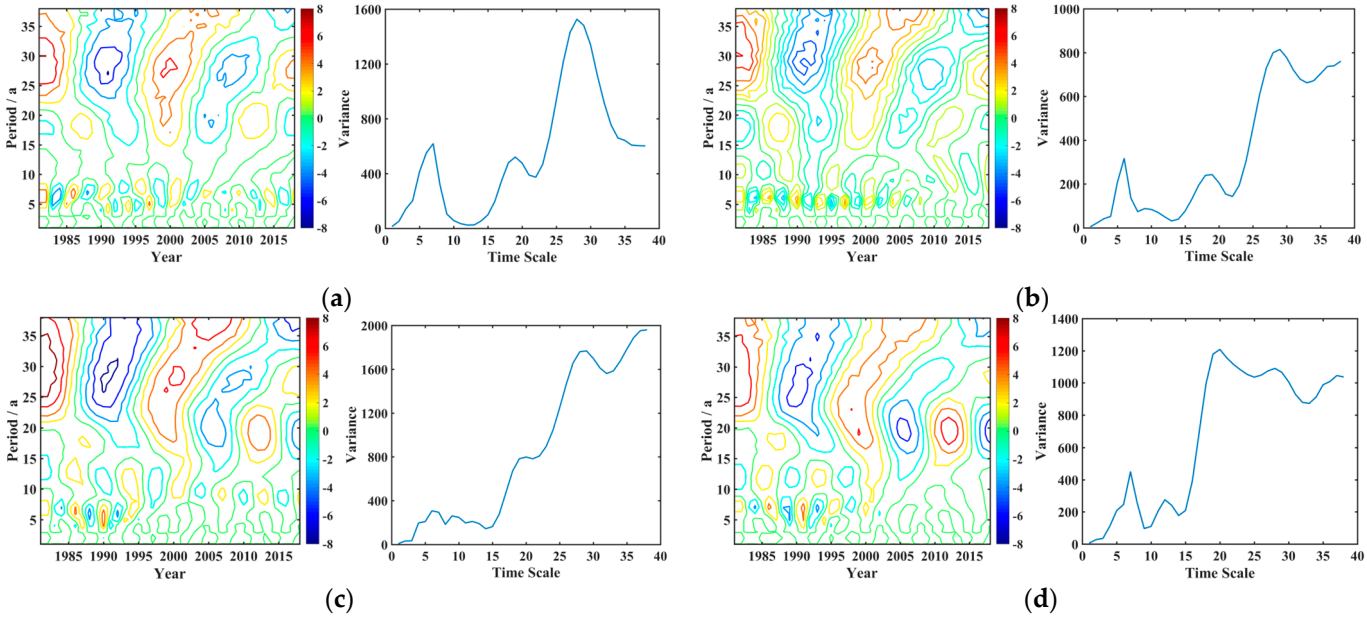

Figure 11. Wavelet time series analysis of NPP in spring (**a**), summer (**b**), autumn (**c**) and winter (**d**). The wavelet coefficient contour map (**left**) and wavelet variance graph (**right**).

5. Discussion

The NPP is an essential part of the terrestrial carbon cycle and represents the atmospheric carbon fixed by vegetation; it is an important indicator of the strength of ecosystem carbon sinks [50]. In this study, the distribution and spatiotemporal dynamics of NPP in Africa from 1981 to 2018 were analyzed. The change trend and fluctuation of annual and seasonal NPP in most regions of Africa were relatively close because Africa is dominated by a tropical rainforest climate, savanna climate, and tropical desert climate, and there is no obvious seasonal change in temperature and precipitation [51,52].

Based on the spatial distribution of precipitation, global land can be segmented into eight arid regions, namely, the Saharan arid region, the Arabian Peninsula arid region, the Central Asia arid region, the Central Mongolian arid region, the North American arid region, the South American arid region, the South African arid region, and the Australian arid region. The arid regions in Africa include the Saharan arid region and the South African arid region [53,54]. Compared with the precipitation in the period from 1901 to 1978, the precipitation in the Saharan arid region decreased by 17.95% from 1979 to 2013, and the precipitation in the South African arid region decreased by 1.29% [53]. The Saharan arid region not only has the largest range but also has a severe degree of drought. Its annual

precipitation is only between 50 and 100 mm, which is close to the conditions of extreme drought. The decrease in precipitation may have a serious impact on the local vegetation. In addition, there is a large population in this region (North Africa to East Asia), and frequent human activities may cause more changes in surface vegetation cover. Consequently, the NPP in the grassland area of the southern Sahara Desert showed a significantly reduced trend and a very high degree of fluctuation [55]. The South African arid area is sparsely populated and has fewer human activities, the arid area is relatively small, and the degree of drought is relatively low. Therefore, although the NPP in this region also showed a significantly reduced trend, it only showed a high degree of fluctuation.

The tropical rainforest is located in the equatorial rainy climate with sufficient annual rainfall. There is no obvious dry or wet season. It is, however, affected by global warming. The NPP in the unspoiled tropical rainforest and other nearby vegetation types basically showed an increasing trend or no significant change and exhibited a low degree of fluctuation [56]. However, the change trend of NPP was not completely synchronous with that of climate. Africa has a large available forest area and a large demand for agriculture and livestock; forest loss in Africa has exceeded 15% in the past 30 years. Africa is the region with the largest amount of deforestation. Approximately four million hectares of forests are cut down or burned every year in Africa, which is roughly equivalent to two times the area of Rwanda [57]. The impact of human activities leads to the expansion of agricultural areas and the destruction of forests and pastures, and a large amount of felling also leads to a reduction in vegetation coverage, resulting in a significant downward trend in NPP in the Congo basin, Gabon, Cameroon, Ghana, Nigeria, Tanzania, and other regions, with a high degree of fluctuation [58–61].

According to the research of Chen et al. [53,56,62], the temperature in Africa experienced a decreasing trend, a rising trend, and a gentle change from 1982 to 2012. During the period from 1982 to 1992, the annual average temperature decreased, while during the period from 1993 to 2002, it increased and then became flat. In general, the temperature increased slightly over 31 years. From 1982 to 2012, the annual precipitation in Africa also showed evidence of a process of decline, rise, decline, and slight change. In general, the annual precipitation decreased [56,62]. In terms of stages, the precipitation dropped sharply from 1989 to 1995 but rose sharply from 1996 to 2000. After 2003, the precipitation basically did not fluctuate much. The analysis of the time series NPP anomaly showed that African NPP can be divided into three stages. The NPP exhibited a downward trend during the period from 1981 to 1992, especially during the period from 1987 to 1992; the NPP grew steadily from 1993 to 2000 and reached its peak in 2000; and the NPP fluctuated from 2001 to 2018, while the abnormally high temperature and drought in 2015 and 2016 caused NPP to be lower than the average level. This result is fundamentally consistent with the variation trend of the above hydrothermal conditions. In addition, the MK analysis results in this study showed that there were obvious mutations in various regions of Africa around 1995, which is related to the sharp changes in hydrothermal conditions that occurred in approximately 1995 in this research.

6. Conclusions

As a key parameter representing terrestrial ecological processes, the NPP of vegetation is an indispensable part of understanding the process of the surface carbon cycle. In this study, we obtained global NPP data from 1981 to 2018 and analyzed the spatiotemporal characteristics of NPP in Africa in the past 38 years. The main conclusions include the following:

1. The NPP of the tropical rainforest and the deciduous broadleaved forest and deciduous needle-leaved forest on the north and south sides of tropical rainforest showed an increasing trend and showed low fluctuations because the tropical rainforest is in the equatorial rainy climate, with sufficient rainfall throughout the year and no obvious dry or wet season. However, the Congo basin, Gabon, Cameroon, Ghana, Nigeria, and Tanzania are affected by human activities, and the NPP in those areas showed

a significant reduced trend and a high degree of fluctuation. The NPP in the Sahara arid area and South Africa arid area showed a significant reduced trend and showed a high degree of fluctuation.

2. From 1981 to 2018, NPP in Africa generally showed a slow upward trend, which can be segmented into three stages. In the declining phase from 1981 to 1992, the NPP was below the average in most years. In the stable growth stage from 1993 to 2000, the NPP peaked in 2000. In the fluctuation stage from 2001 to 2018, the NPP value was above average in all years except 2015 and 2016, when the NPP value was low due to abnormally high temperatures and drought. The Mann–Kendall test further showed that the variation in NPP in Africa followed a true rising trend, rather than a random fluctuation, and the annual and seasonal changes reached a significant level. The year and season had one mutation point within the confidence interval in 1994, 1995, 1992, 1993, and 1994.
3. On an annual scale, Africa obviously has short cycles of 4 to 8 years, 15 to 21 years, and 23 to 35 years and long cycles of 42 to 62 years, while the annual and seasonal NPPs have obvious oscillations on timescales of 7 years, 20 years, 29 years, and 55 years. Among them, the 55-year period had the strongest signal, which was the first primary period. The second main cycle was different from the third main cycle.

Author Contributions: Conceptualization, L.L.; methodology, L.L. and Q.W.; software, Q.W. and L.L.; validation, L.L. and Q.W.; formal analysis, L.L. and Q.W.; investigation, L.L., Q.W., J.S. and C.S.; resources, L.L. and Q.W.; data curation, Q.W. and L.L.; writing—original draft preparation, Q.W. and L.L.; writing—review and editing, L.L., Q.W., S.W. (Shuguo Wang), S.W. (Sisi Wang), L.Z., S.Q. and Y.S.; visualization, Q.W. and L.L.; supervision, L.L.; project administration, L.L.; funding acquisition, L.L. and L.Z. All authors have read and agreed to the published version of the manuscript.

Funding: This research was funded by the National Natural Science Foundation of China (No. 41971305), the China Europe Dragon 5 Cooperation Programme (No. 59197), the Double Carbon Project of Jiangsu Normal University (JSNUSTZX202202), the Postgraduate Research and Practice Innovation Program of Jiangsu Province (KYCX22_2849, SJCX21_1128), the Postgraduate Research and Practice Innovation Program of Jiangsu Normal University (2022XKT0067, 2022XKT0125), the Project Funded by the Priority Academic Program Development of Jiangsu Higher Education Institutions (PAPD).

Data Availability Statement: Data may be provided on reasonable request to corresponding author.

Acknowledgments: Acknowledgement for the data support from "National Earth System Science Data Center, National Science & Technology Infrastructure of China. (http://www.geodata.cn)".

Conflicts of Interest: The authors declare no conflict of interest.

References

1. Liu, J.; Chen, J.M.; Cihlar, J.; Chen, W. Net primary productivity distribution in the BOREAS region from a process model using satellite and surface data. *J. Geophys. Res.-Atmos.* **1999**, *104*, 27735–27754. [CrossRef]
2. Field, C.B.; Behrenfeld, M.J.; Randerson, J.T.; Falkowski, P. Primary Production of the Biosphere: Integrating Terrestrial and Oceanic Components. *Science* **1998**, *281*, 237–240. [CrossRef]
3. IGBP Terrestrial Carbon Working Group. The Terrestrial Carbon Cycle: Implications for the Kyoto Protocol. *Science* **1998**, *280*, 1393–1394. [CrossRef]
4. Cai, X.M. *The Ecology of Ecosystem*; Science Press: Beijing, China, 2000.
5. Cui, J.B.; Li, C.S.; Trettin, C. Analyzing the ecosystem carbon and hydrologic characteristics of forested wetland using a biogeochemical process model. *Glob. Chang. Biol.* **2005**, *11*, 278–289. [CrossRef]
6. Lieth, H. Primary Production: Terrestrial Ecosystems. *Hum. Ecol.* **1973**, *1*, 303–332. [CrossRef]
7. Seino, H.S.; Uchijima, Z.B. Global Distribution of Net Primary Productivity of Terrestrial Vegetation. *J. Agric. Meteorol.* **1992**, *48*, 39–48. [CrossRef]
8. Parton, W.J.; Stewart, J.W.B.; Cole, C.V. Dynamics of C, N, P and S in Grassland Soils: A Model. *Biogeochemistry* **1988**, *5*, 109–131. [CrossRef]
9. Running, S.W.; Hunt, E.R. 8—Generalization of a Forest Ecosystem Process Model for Other Biomes, BIOME-BGC, and an Application for Global-Scale Models. In *Scaling Physiological Processes*; Ehleringer, J.R., Field, C.B., Eds.; Academic Press: San Diego, CA, USA, 1993; pp. 141–158.

10. Potter, C.S.; Randerson, J.T.; Field, C.B.; Matson, P.A.; Vitousek, P.M.; Mooney, H.A.; Klooster, S.A. Terrestrial ecosystem production: A process model based on global satellite and surface data. *Glob. Biogeochem. Cycles* **1993**, *7*, 811–841. [CrossRef]
11. Prince, S.D.; Goward, S.N.; Hanan, N.P. Estimation of Global Primary Production Using NOAA/NASA Pathfinder AVHRR Land Data Set. *Igarss* **1995**, *2*, 1000–1002.
12. Hong, C.Q.; Jin, X.B.; Chen, C.C.; Wang, S.M.; Yang, X.H.; Xiang, X.M. Overview on estimation models of land net primary productivity integrating remote sensing data. *Prog. Geogr.* **2017**, *36*, 924–939.
13. Liu, J.; Chen, J.M.; Cihlar, J.; Chen, W.; Park, W.M. A process-based boreal ecosystem productivity simulator using remote sensing inputs. *Remote Sens. Environ.* **1997**, *62*, 158–175. [CrossRef]
14. Matsushita, B.; Tamura, M. Integrating remotely sensed data with an ecosystem model to estimate net primary productivity in East Asia. *Remote Sens. Environ.* **2002**, *81*, 58–66. [CrossRef]
15. Qiu, S.Y.; Liang, L.; Wang, Q.J.; Geng, D.; Wu, J.J.; Wang, S.G.; Chen, B.Q. Estimation of European Terrestrial Ecosystem NEP Based on an Improved CASA Model. *IEEE J.-Stars.* **2023**, *16*, 1244–1255. [CrossRef]
16. Mao, J.F.; Wang, B.; Dai, Y.J.; Woodward, F.I.; Hanson, P.J.; Lomas, M.R. Improvements of a dynamic global vegetation model and simulations of carbon and water at an upland-oak forest. *Adv. Atmos. Sci.* **2007**, *24*, 311–322. [CrossRef]
17. Gulbeyaz, O.; Bond-Lamberty, B.; Akyurek, Z.; West, T.O. A new approach to evaluate the MODIS annual NPP product (MOD17A3) using forest field data from Turkey. *Int. J. Remote Sens.* **2018**, *39*, 2560–2578. [CrossRef]
18. Ghaderpour, E.; Mazzanti, P.; Mugnozza, G.S.; Bozzano, F. Coherency and phase delay analyses between land cover and climate across Italy via the least-squares wavelet software. *Int. J. Appl. Earth Obs.* **2023**, *118*, 103241. [CrossRef]
19. Aalijahan, M.; Karatas, A.; Lupo, A.R.; Efe, B.; Khosravichenar, A. Analyzing and Modeling the Spatial-Temporal Changes and the Impact of GLOTI Index on Precipitation in the Marmara Region of Turkiye. *Atmosphere* **2023**, *14*, 489. [CrossRef]
20. Liang, L.; Qiu, S.Y.; Yan, J.; Shi, Y.Y.; Geng, D. VCI-Based Analysis on Spatiotemporal Variations of Spring Drought in China. *Int. J. Environ. Res. Public Health* **2021**, *18*, 7967. [CrossRef]
21. Castañeda-Moya, E.; Twilley, R.R.; Rivera-Monroy, V.H. Allocation of biomass and net primary productivity of mangrove forests along environmental gradients in the Florida Coastal Everglades, USA. *For. Ecol. Manag.* **2013**, *307*, 226–241. [CrossRef]
22. Eisfelder, C.; Klein, I.; Niklaus, M.; Kuenzer, C. Net primary productivity in Kazakhstan, its spatio-temporal patterns and relation to meteorological variables. *J. Arid Environ.* **2014**, *103*, 17–30. [CrossRef]
23. Liang, L.; Di, L.P.; Zhang, L.P.; Deng, M.X.; Qin, Z.H.; Zhang, S.H.; Lin, H. Estimation of crop LAI using hyperspectral vegetation indices and a hybrid inversion method. *Remote Sens. Environ.* **2015**, *165*, 123–134. [CrossRef]
24. Chen, F.J.; Shen, Y.J.; Li, Q.; Guo, Y.; Xu, L.M. Spatio-temporal Variation Analysis of Ecological Systems NPP in China in Past 30 years. *Sci. Geogr. Sin.* **2011**, *31*, 1409–1414.
25. Liang, L.; Di, L.P.; Huang, T.; Wang, J.H.; Li, L.; Wang, L.J.; Yang, M.H. Estimation of Leaf Nitrogen Content in Wheat Using New Hyperspectral Indices and a Random Forest Regression Algorithm. *Remote Sens.* **2018**, *10*, 1940. [CrossRef]
26. Lu, G.; Han, M.; Xu, Z.H.; Zhu, J.Q.; Niu, X.R. Spatiotemporal variations of net primary productivity in new wetlands of the Yellow River Delta. *Chin. J. Ecol.* **2019**, *38*, 1113–1122.
27. Jin, Y.; Lin, Q.N.; Mao, S.P. Challenges and Countermeasures for Deepening China-Africa Agricultural Investment Cooperation. *Intertrade* **2022**, *10*, 19–26.
28. Zhan, S.M. To Meet Climate Changes: The African Stance and Concerns. *West Asia Afr.* **2009**, *10*, 42–49+80.
29. Statistics Division, United Nations. Available online: https://unstats.un.org/unsd/methodology/m49/ (accessed on 15 October 2022).
30. Statistics Division, United Nations. *Standard Country or Area Codes for Statistical Use*; United Nations: New York, NY, USA, 1999.
31. ONU. *World Statistics Pocketbook 2019*; United Nations: New York, NY, USA, 2019.
32. Liu, L.Y.; Bai, Y.; Sun, R.; Niu, Z.G. Stereo Observation and Inversion of the Key Parameters of Global Carbon Cycle: Project Overview and Mid-Term Progressess. *Remote Sens. Technol. Appl.* **2021**, *36*, 11–24.
33. Yu, T.; Sun, R.; Xiao, Z.Q.; Zhang, Q.; Liu, G.; Cui, T.X.; Wang, J.M. Estimation of Global Vegetation Productivity from Global Land Surface Satellite Data. *Remote Sens.* **2018**, *10*, 327. [CrossRef]
34. National Earth System Science Data Center, National Science & Technology Infrastructure of China. Available online: http://www.geodata.cn.
35. Congalton, R.G.; Gu, J.Y.; Yadav, K.; Thenkabail, P.; Ozdogan, M. Global Land Cover Mapping: A Review and Uncertainty Analysis. *Remote Sens.* **2015**, *6*, 12070–12093. [CrossRef]
36. Yang, R.F.; Yin, S.Y. Analysis of the variation of NPP and its responses with climate changes of global tropical forests. *Acta Ecol. Sin.* **2019**, *39*, 8504–8515.
37. Liang, L.; Geng, D.; Yan, J.; Qiu, S.Y.; Shi, Y.Y.; Wang, S.G.; Wang, L.J.; Zhang, L.P.; Kang, J.R. Remote Sensing Estimation and Spatiotemporal Pattern Analysis of Terrestrial Net Ecosystem Productivity in China. *Remote Sens.* **2022**, *14*, 1902. [CrossRef]
38. Li, Y.; Wang, Y.F.; Sun, Y.J.; Lei, Y.C.; Shao, W.C.; Li, J. Temporal-spatial characteristics of NPP and its response to climate change of Larix forests in Jilin Province. *Acta Ecol. Sin.* **2022**, *42*, 947–959.
39. Wang, F.; Wang, Z.; Zhang, Y. Spatio-temporal Variations in Vegetation Net Primary Productivity and Their driving Factors in Anhui Province from 2000 to 2015. *Acta Ecol. Sin.* **2018**, *38*, 2754–2767.
40. Guo, Z.X.; Wang, Z.M.; Liu, D.W.; Song, K.S.; Song, C.C. Analysis of temporal and spatial features of farmland productivity in the Sanjiang Plain. *Trans. CSA* **2009**, *25*, 249–254.

41. Wei, F.Y. *Statistical Diagnosis and Prediction Technology of Modern Climate*; China Meteorological Press: Beijing, China, 1999.
42. Mallick, J.; Talukdar, S.; Alsubih, M.; Salam, R.; Ahmed, M.; Kahla, N.B.; Shamimuzzaman, M. Analysing the trend of rainfall in Asir region of Saudi Arabia using the family of Mann-Kendall tests, innovative trend analysis, and detrended fluctuation analysis. *Theor. Appl. Climatol.* **2020**, *143*, 823–841. [CrossRef]
43. Sneyers, R. On the Statistical Analysis of Series of Observations. *Technical. Note* **1990**, *143*. Available online: https://www.researchgate.net/publication/309122890_On_the_statistical_analysis_of_series_of_observations (accessed on 21 May 2023).
44. Liang, L.; Sun, Q.; Luo, X.; Wang, J.H.; Zhang, L.P.; Deng, M.X.; Di, L.P.; Liu, Z.X. Long-term spatial and temporal variations of vegetative drought based on vegetation condition index in China. *Ecosphere* **2017**, *8*, e01919. [CrossRef]
45. Fu, C.B.; Wang, Q. Definition and detection methods of abrupt climate change. *Sci. Atmos. Sinica* **1992**, *16*, 482–493.
46. Torrence, C.; Compo, G.P. A practical guide to wavelet analysis. *B Am. Meteorol. Soc.* **1998**, *79*, 61–78. [CrossRef]
47. Liu, Y.; Xu, G.; Yin, Z.; Hu, C.; Wang, Y.; Liao, F. Spatio-temporal change of surface air temperature in Anhui province in the context of global warming from 1960 to 2014. *J. Nat. Resour.* **2017**, *32*, 680–691.
48. Lara, C.; Saldías, G.S.; Paredes, A.L.; Cazelles, B.; Broitman, B.R. Temporal Variability of MODIS Phenological Indices in the Temperate Rainforest of Northern Patagonia. *Remote Sens.* **2018**, *10*, 956. [CrossRef]
49. Wanders, N.; Bachas, A.; He, X.G.; Huang, H.; Koppa, A.; Mekonnen, Z.T.; Pagán, B.R.; Peng, L.Q.; Vergopolan, N.; Wang, K.J.; et al. Forecasting the hydroclimatic signature of the 2015-16 El Niño event on the western U.S. *J. Hydrometeorol.* **2017**, *18*, 177–186. [CrossRef]
50. Zhao, X.J.; Wu, W.J.; Liu, G.L. Analysis of Global NPP Variation Pattern Using Data Driven Method. *Remote Sens. Inf.* **2019**, *34*, 26–33.
51. Yao, G.M. The Roots of Agricultural Crisis in Africa. *West Asia Afr.* **2002**, *3*, 22–25+79.
52. Shi, Y.J. Study on Innovation of Agricultural Cooperation Model Between China and African Countries. Ph.D. Thesis, Shihezi University, Shihezi, China, 2009.
53. Zuo, B. Development of a New Detection Method for Climate Trend Turning and the Spatial-Temporal Characteristics of Global Surface Air Temperature Trend Turnings. Ph.D. Thesis, Lanzhou University, Lanzhou, China, 2019.
54. Li, Y. Study on Global Semi-Arid Climate Change. Ph.D. Thesis, Lanzhou University, Lanzhou, China, 2015.
55. Yang, Z.F.; Qi, Y.L.; Wu, Z.X. Variation characteristics of global dryland temperature and precipitation in the past 60 years. *Gansu Sci. Technol.* **2018**, *34*, 23–27.
56. Chen, S.Y. Study on the Response Mechanism of Main Vegetation Types Growth Variation to Climate Change in Africa Based on GLASS-LAI. Master's Thesis, Nanjing University, Nanjing, China, 2016.
57. Wang, T.; Wang, M. The Current Situation, Opportunities and Challenges of Low-Carbon Development in Africa. *J. Southwest Pet. Univ. (Soc. Sci. Ed.)* **2015**, *17*, 1–9.
58. Kankeu, R.S.; Sonwa, D.J.; Atyi, I.E.; Nkal, N.M.M. Quantifying post logging biomass loss using satellite images and ground measurements in Southeast Cameroon. *J. For. Res.* **2016**, *27*, 1415–1426. [CrossRef]
59. Perez, M.R.; de Blas, D.E.; Nasi, R.; Sayer, J.A.; Sassen, M.; Angoue, C.; Gami, N.; Ndoye, O.; Ngono, G.; Nguinguiri, J.C.; et al. Logging in the Congo Basin: A multi-country characterization of timber companies. *For. Ecol. Manag.* **2005**, *214*, 221–236. [CrossRef]
60. Antropov, O.; Rauste, Y.; Praks, J.; Seifert, F.; Hame, T. Mapping Forest Disturbance Due to Selective Logging in the Congo Basin with RADARSAT-2 Time Series. *Remote Sens.* **2021**, *13*, 740. [CrossRef]
61. Sona, M.F.M. Classification and Net Primary Productivity of Potential Natural Vegetation in Africa Continent from 1911 to 2013. Ph.D. Thesis, Northwest Normal University, Lanzhou, China, 2016.
62. Chen, J.; Zhang, Y.C.; Cihlar, J.; Chen, W. Regional differences of land extreme precipitation and temperature changes under climate change condition. *Plateau Meteor.* **2016**, *35*, 955–968.